Spatio-angular transfer functions for fluorescence microscopes

Talon Chandler, Min Guo, Hari Shroff, Rudolf Oldenbourg, Patrick La Rivière

March 3, 2018

Abstract

We investigate how the orientation and position of fluorescent dipole emitters affects microscopic imaging using electromagnetic optics theory. Starting with the thoroughly studied spatio-angular point spread function, we introduce the spatio-angular coherent spread function, coherent transfer function, and optical transfer function as electromagnetic counterparts to well-known functions in scalar optics theory. We use these concepts to show that fluorescence microscopes have a spatio-angular band limit. Finally, we study polarized light microscopes and find that polarized illumination is a type of structured illumination that extends the angular band limit.

1 Introduction

TODO

We use plain roman type for scalars, e.g., x, y, z; bold lowercase roman type for two-dimensional vectors, e.g., $\mathbf{r}$; hats for unit vectors, e.g., $\hat{\mathbf{s}}$; bold lowercase gothic type for three-dimensional vectors, e.g., $\mathfrak{r}$; and bold capital roman type for matrices, e.g., $\mathbf{R}$.

2 General forward model

Consider a three-dimensional field of oriented fluorescent dipoles. We can represent the entire field using a function $f(\mathfrak{r}_o, \hat{\mathbf{s}}_o)$ that returns the number of dipoles at position $\mathfrak{r}_o$ per unit volume oriented in direction $\hat{\mathbf{s}}_o$ per unit solid angle. We call $f(\mathfrak{r}_o, \hat{\mathbf{s}}_o)$ the fluorescence spatio-angular density because it has units of fluorophores per volume per solid angle.

If each fluorophore in the field fluoresces independently then the measured intensity is a weighted sum of the intensity contributions from each fluorophore, and we can model the imaging system with

$$g_i(\mathbf{r}_d) = \int_{\mathbb{R}^3} d\mathfrak{r}_o \int_{\mathbb{S}^2} d\hat{\mathbf{s}}_o \; h_i(\mathbf{r}_d; \mathfrak{r}_o, \hat{\mathbf{s}}_o) f(\mathfrak{r}_o, \hat{\mathbf{s}}_o) \tag{1}$$

where $g_i(\mathbf{r_d})$ are the intensities measured by the detector under the ith measurement configuration (i can index polarizer settings or views), $\mathbf{r_d}$ is the two-dimensional detector coordinate, and $h_i(\mathbf{r}_d; \mathfrak{r}_o, \hat{\mathbf{s}}_o)$ is the spatio-angular point spread function (PSF) of the ith measurement configuration. Our goal is to reconstruct the object $f(\mathfrak{r}_o, \hat{\mathbf{s}}_o)$ from intensity measurements $g_i(\mathbf{r}_d)$.

We can also use the spatio-angular density to model translating and rotating fluorophores. As long as each fluorescence emission is an independent event, then equation 1 is a valid way to model the imaging system.

3 Spatio-angular point spread function

Figure 3 shows a schematic of the fluorescence microscope that we are considering with a summary of our notation. We start by following Backer and Moerner [1] to find the electric field in the back focal plane due to a single dipole emitter at position $\mathfrak{r}_o$ oriented along $\hat{\mathbf{s}}_o$ as

$$\mathbf{e_b}(\mathbf{r}_b; \mathfrak{r}_o, \hat{\mathbf{s}}_o) \propto \mathrm{e}^{in_o k(z_o \rho_b)} \sqrt{\frac{1}{\rho_b}} \begin{bmatrix} \sin^2\phi_b + \rho_b \cos^2\phi_b & \sin\phi_b \cos\phi_b(\rho_b - 1) & -r_b \cos\phi_b \\ \sin\phi_b \cos\phi_b(\rho_b - 1) & \cos^2\phi_b + \rho_b \sin^2\phi_b & -r_b \sin\phi_b \\ 0 & 0 & 0 \end{bmatrix} \begin{bmatrix} \cos\varphi_o \sin\vartheta_o \\ \sin\varphi_o \sin\vartheta_o \\ \cos\vartheta_o \end{bmatrix} \Pi\left(\frac{r_b}{r_b^{\max}}\right) \tag{2}$$

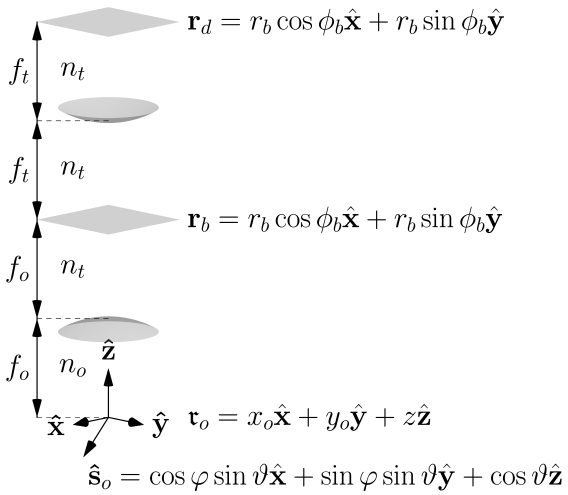

Figure 1: Simplified schematic of a single-view fluorescence microscope. The object is placed near the focal point of an aplanatic objective lens with focal length f_o in a medium with refractive index n_o. The object is parameterized by the 3D position vector $\mathfrak{r}_o$ (o for object) and an orientation unit vector $\hat{\mathbf{s}}_o$. The light emitted by the fluorescent object is collected and collimated by the objective lens so that the electric fields are purely transverse in the back focal plane. Points in the back focal plane are parameterized by a 2D position vector $\mathbf{r}_b$ (b for back focal plane). Finally, the tube lens with focal length f_t refocuses the light onto a detector. Points on the detector are parameterized by a 2D position vector $\mathbf{r}_d$ (d for detector). The back focal plane and detector are in a medium with refractive index n_t. Note that this schematic is not to scale—we consider the case where $f_o \ll f_t$.

where we have defined $\rho_b \equiv \sqrt{1 - r_b^2}$ and $\Pi(x)$ is a boxcar function that returns 1 when $|x| < 1$ and 0 otherwise. We can understand this expression term by term—the exponential term accounts for the defocus phase, the square root term conserves power before and after the objective lens, the matrix models the dipole emission process and electric field rotation caused by the objective lens, the vector is the dipole orientation unit vector, and $\Pi\left(\frac{r_b}{r_b^{\max}}\right)$ accounts for the numerical aperture of the lens with $r_b^{\max} = \frac{f_0}{n_0}\text{NA}$. Notice that we have omitted the dependence on the transverse position of the fluorophore x_o and y_o. This is because we assume that the objective is aplanatic, so it displays transverse shift-invariance and the constant phase factor does not affect our discussion.

We can find the intensity in the detector plane by propagating the electric field to the detector plane using a scaled Fourier transform then taking the modulus squared

$$h_i(\mathbf{r}_d; \mathfrak{r}_o, \hat{\mathbf{s}}_o) = \left| \int_{\mathbb{R}^2} d\mathbf{r}_b \mathbf{e}_b(\mathbf{r}_b; \mathfrak{r}_o, \hat{\mathbf{s}}_o) \mathrm{e}^{-i(kn_t/f_t)\mathbf{r}_b \cdot \mathbf{r}_d} \right|^2 . \tag{3}$$

Following Novotny [2], we write the Fourier transform in polar coordinates, evaluate the azimuthal integrals, and write the result concisely in terms of three radial integrals

$$h_i(\mathbf{r}_d; \mathfrak{r}_o, \hat{\mathbf{s}}_o) = \left| \mathbf{e}_d(\mathbf{r}_d; \mathfrak{r}_o, \hat{\mathbf{s}}_o) \right|^2 . \tag{4}$$

$$\mathbf{e}_d(\mathbf{r}_d; \mathfrak{r}_o, \hat{\mathbf{s}}_o) \propto \begin{bmatrix} I_0 + I_2 \cos(2\phi_d) & I_2 \sin(2\phi_d) & -2iI_1 \cos\phi_d \\ I_2 \sin(2\phi_d) & I_0 - I_2 \cos(2\phi_d) & -2iI_1 \sin\phi_d \\ 0 & 0 & 0 \end{bmatrix} \begin{bmatrix} \cos\varphi_o \sin\vartheta_o \\ \sin\varphi_o \sin\vartheta_o \\ \cos\vartheta_o \end{bmatrix} \tag{5}$$

where I_0, I_1 and I_2 are

$$I_0(r_d; z_o) = \int_0^{\theta_{\max}} d\theta \ \sqrt{\cos\theta}\sin\theta(1+\cos\theta)J_0(k_b r_d \sin\theta f_o/f_t) \ \exp\left\{ik_b z_o[1-(1/2)(f_o/f_t)^2\sin^2\theta]\right\}, \tag{6}$$

$$I_1(r_d; z_o) = \int_0^{\theta_{\max}} d\theta \ \sqrt{\cos\theta}\sin^2\theta J_1(k_b r_d \sin\theta f_o/f_t) \ \exp\left\{ik_b z_o[1-(1/2)(f_o/f_t)^2\sin^2\theta]\right\}, \tag{7}$$

$$I_2(r_d; z_o) = \int_0^{\theta_{\max}} d\theta \ \sqrt{\cos\theta}\sin\theta(1-\cos\theta)J_2(k_b r_d \sin\theta f_o/f_t) \ \exp\left\{ik_b z_o[1-(1/2)(f_o/f_t)^2\sin^2\theta]\right\}. \tag{8}$$

By plugging Eq. 5 into equation Eq. 4 and expanding in terms of the spherical harmonic functions, we can rewrite the spatio-angular PSF as

$$\begin{aligned} h(\mathbf{r}_d; \mathfrak{r}_o, \hat{\mathbf{s}}_o) \propto & \frac{4\sqrt{\pi}}{3}\left(I_0^2 + 2I_1^2 + I_2^2\right) Y_0^0(\hat{\mathbf{s}}_o) - \frac{8\sqrt{15\pi}}{15} I_0 I_2 \sin(2\phi_d) Y_2^{-2}(\hat{\mathbf{s}}_o) \\ & + \frac{4\sqrt{5\pi}}{15}\left(-I_0^2 + 4I_1^2 - I_2^2\right) Y_2^0(\hat{\mathbf{s}}_o) + \frac{8\sqrt{15\pi}}{15} I_0 I_2 \cos(2\phi_d) Y_2^{-2}(\hat{\mathbf{s}}_o). \end{aligned} \tag{9}$$

We have chosen to write the spatio-angular PSF in terms of spherical harmonic functions for two reasons. First, it allows us to express the spatio-angular PSF very concisely. Instead of considering the point spread function for every possible dipole orientation, we only need to consider four spatio-angular PSFs—one for each spherical harmonic. Second, the spherical harmonic functions form an orthonormal basis for functions on the sphere—a convenient fact that we will use later.

It is useful to compare equation 9 to Backer and Moerner's approach [1]. They expand the spatio-angular PSF in terms of six second moments of the fluorophore distribution $\{s_x^2, s_y^2, s_z^2, s_x s_y, s_x s_z, s_y s_z\}$. This approach is very useful—only six precomputed spatio-angular PSFs are required to represent an arbitrary spatio-angular PSF. Instead of expanding in terms of six second moments, we expand onto just four spherical harmonics which, unlike the second moments, are orthonormal functions. In the next section we will use the orthonormality of the spherical harmonics to derive spatio-angular transfer functions for fluorescence microscopes.

For now, let's look closer at the spatio-angular PSF in a special case. By constraining the object to the focal plane ($z_o = 0$) and applying the paraxial approximation ($\sin\theta \approx \theta$ and $\cos\theta \approx 1$), the integrals I_{0-2} can be evaluated in terms of Bessel functions. We can evaluate I_0 and I_1 with the help of $\int_0^z dx \ xJ_0(ax) = zJ_1(az)/a$ and $\int_0^z dx \ x^2 J_1(ax) = z^2 J_2(az)/a$, respectively, and $I_2 = 0$ because $J_2(x)$ is zero to first order. In this case, the spatio-angular PSF simplifies to

$$\lim_{\theta_{\max} \ll \pi/2} h(\mathbf{r}_d; \mathbf{r}_o, z_o = 0, \hat{\mathbf{s}}_o) \equiv h^*(\mathbf{r}_d; \mathbf{r}_o, \hat{\mathbf{s}}_o) \propto \frac{4\sqrt{\pi}}{3}(I_0^{*2} + 2I_1^{*2}) Y_0^0(\hat{\mathbf{s}}_o) + \frac{4\sqrt{5\pi}}{15}\left(-I_0^{*2} + 4I_1^{*2}\right) Y_2^0(\hat{\mathbf{s}}_o) \tag{10}$$

where the integrals evaluate to

$$I_0^* = \left(\frac{\mathrm{NA}}{n_o}\right)^2 \left[\frac{2J_1(\tilde{r}_d)}{\tilde{r}_d}\right], \qquad I_1^* = \left(\frac{\mathrm{NA}}{n_o}\right)^3 \left[\frac{2J_2(\tilde{r}_d)}{\tilde{r}_d}\right], \tag{11}$$

and we have substituted

$$\tilde{r}_d = \frac{2\pi \mathrm{NA}\, r_d}{M\lambda}, \qquad \mathrm{NA} = n_o \sin\theta_{\max}, \qquad M = \frac{n_o}{n_b}\frac{f_t}{f_o}. \tag{12}$$

We will continue to use an asterisk to mark the terms where we have used the paraxial approximation and constrained the object to the focal plane.

First, consider the coefficient on the Y_0^0 spherical harmonic in Eq. 10. This coefficient is the point spread function for a angularly uniform distribution of fluorophores. The first term of the coefficient I_0^* is the familiar

Airy disk that arises from the contribution of dipoles oriented in the transverse plane, while the second term I_1^* is a smaller factor that arises from dipoles oriented outside of the transverse plane. This leads to an interesting conclusion—a uniform distribution of dipoles has a point spread function that is slightly wider than an Airy disk even in the paraxial approximation. The Airy disk is usually derived using paraxial scalar optics while here we have used paraxial electromagnetic optics. Therefore, we can consider the second term to be an electromagnetic correction to the Airy disk. We will quantify this difference in the next section.

Next, consider the coefficient on the Y_2^0 spherical harmonic in Eq. 10. This coefficient is the spatial PSF for a distribution of fluorophores proportional to $3\cos^2\vartheta_o - 1$. Counterintuitively, this fluorophore distribution cannot exist because it would require a negative number of fluorophores along some orientations; but if this distribution could exist, then this coefficient would be its spatial PSF. Considering negative distributions of fluorophores in our calculations should not be cause for concern. The spherical harmonics span the space of functions on the sphere, so any positive fluorophore distribution can be represented by the spherical harmonics and we never need to consider negative fluorophores.

Finally, consider all of the spherical harmonics that have a zero coefficient. These spherical harmonics span the angular null space of our measurement system—fluorophore distributions that lie in the null space do not affect the measured intensities. Under the paraxial approximation all of the non-zero coefficients are rotationally symmetric ($m = 0$) spherical harmonics which means that the transverse orientation of the dipoles does not affect the PSF. In the high NA case this is no longer true—two $m = 2$ spherical harmonics have non-zero coefficients and the transverse orientation of dipoles does affect the PSF.

4 Spatio-angular transfer functions

We define the spatio-angular optical transfer function (OTF) as

$$H_l^m(\boldsymbol{\nu}_o) = \int_{\mathbb{R}^3} d\mathfrak{r}_o \int_{\mathbb{S}^2} d\hat{\mathbf{s}}_o \; h_i(\mathbf{r}_d; \mathfrak{r}_o, \hat{\mathbf{s}}_o) Y_l^m(\hat{\mathbf{s}}_o)\, \mathrm{e}^{i2\pi\mathfrak{r}_o\cdot\boldsymbol{\nu}_o}. \tag{13}$$

The spatio-angular OTF measures the ability of the microscope to pass spatio-angular harmonics—instead of the usual spatial harmonics $\mathrm{e}^{i2\pi\mathfrak{r}_o\cdot\boldsymbol{\nu}_o}$ we now need consider the spatio-angular harmonics $Y_l^m(\hat{\mathbf{s}}_o)\,\mathrm{e}^{i2\pi\mathfrak{r}_o\cdot\boldsymbol{\nu}_o}$. Eq. 13 can be interpreted as the spatio-angular Fourier transform of the spatio-angular PSF.

We can plug Eq. 9 into 13 and use the orthonormality relation for spherical harmonics $\int_{\mathbb{S}^2} d\hat{\mathbf{s}}_o Y_{l_0}^{m_0}(\hat{\mathbf{s}}_o) Y_{l_1}^{m_1}(\hat{\mathbf{s}}_o) = \delta(l_0 - l_1)\delta(m_0 - m_1)$ to find that

$$\begin{aligned} H_l^m(\boldsymbol{\nu}_o) \propto \int_{\mathbb{R}^3} d\mathfrak{r}_o & \frac{4\sqrt{\pi}}{3}\left(I_0^2 + 2I_1^2 + I_2^2\right)\delta(l)\delta(m) \\ & - \frac{8\sqrt{15\pi}}{15} I_0 I_2 \sin(2\phi_d)\,\delta(l-2)\delta(m+2) \\ & + \frac{4\sqrt{5\pi}}{15}\left(-I_0^2 + 4I_1^2 - I_2^2\right)\delta(l-2)\delta(m) \\ & + \frac{8\sqrt{15\pi}}{15} I_0 I_2 \cos(2\phi_d)\,\delta(l-2)\delta(m-2). \end{aligned} \tag{14}$$

We can see that the microscope has an angular band limit—the microscope only passes intensity contributions for fluorophore distributions in the $l = 0$ and $l = 2$ bands.

Once again, we constrain the object to the focal plane and apply the paraxial approximation to find that

$$H_l^{m*}(\nu_o^x, \nu_o^y) \propto \int_{\mathbb{R}^2} d\mathbf{r}_o \left[\frac{4\sqrt{\pi}}{3}(I_0^{*2} + 2I_1^{*2})\delta(l)\delta(m) + \frac{4\sqrt{5\pi}}{15}\left(-I_0^{*2} + 4I_1^{*2}\right)\delta(l-2)\delta(m)\right] \mathrm{e}^{i2\pi(\nu_o^x x_o + \nu_o^y y_o)} \tag{15}$$

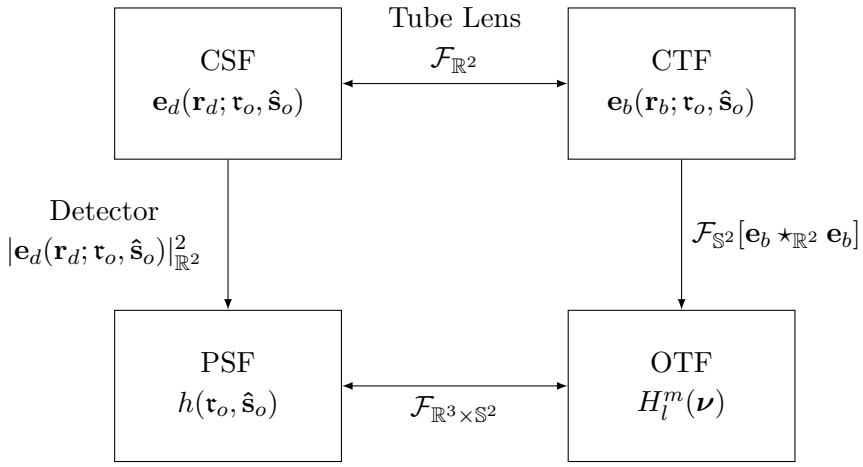

Figure 2: Summary of relationships between the CSF, CTF, PSF, and OTF where $\mathcal{F}_D$, $|\cdot|_D$, and $\star_D$ denote the Fourier transform, norm, and autocorrelation over the set D, respectively. See [3] and [5] for analogous diagrams under scalar optics approximations.

The integrals in Eqs. 14 and 15 cannot be solved directly. We could proceed numerically like [1], but instead we use the Wiener-Khinchin theorem to simplify the integral [3, 4]. We plug Eq. 3 into Eq. 13

$$H_l^m(\boldsymbol{\nu}_o) = \int_{\mathbb{R}^3} d\mathfrak{r}_o \int_{\mathbb{S}^2} d\hat{\mathbf{s}}_o \left| \int_{\mathbb{R}^2} d\mathbf{r}_b \mathbf{e}_b(\mathbf{r}_b; \mathfrak{r}_o, \hat{\mathbf{s}}_o) \mathrm{e}^{-i(kn_t/f_t)\mathbf{r}_b \cdot \mathbf{r}_d} \right|^2 Y_l^m(\hat{\mathbf{s}}_o)\, \mathrm{e}^{i2\pi \mathfrak{r}_o \cdot \boldsymbol{\nu}_o}, \tag{16}$$

change the order of the integrals

$$H_l^m(\boldsymbol{\nu}_o) = \int_{\mathbb{S}^2} d\hat{\mathbf{s}}_o\, Y_l^m(\hat{\mathbf{s}}_o) \int_{\mathbb{R}^3} d\mathfrak{r}_o \left| \int_{\mathbb{R}^2} d\mathbf{r}_b \mathbf{e}_b(\mathbf{r}_b; \mathfrak{r}_o, \hat{\mathbf{s}}_o) \mathrm{e}^{-i(kn_t/f_t)\mathbf{r}_b \cdot \mathbf{r}_d} \right|^2 \mathrm{e}^{i2\pi \mathfrak{r}_o \cdot \boldsymbol{\nu}_o},$$

and apply the Wiener-Khinchin theorem $\mathcal{F}\{|\mathcal{F}\{\mathbf{e}_b\}|^2\} = \mathbf{e}_b \star \mathbf{e}_b$ to find that

$$H_l^m(\boldsymbol{\nu}_o) = \int_{\mathbb{S}^2} d\hat{\mathbf{s}}_o\, Y_l^m(\hat{\mathbf{s}}_o)\, [\mathbf{e}_b \star \mathbf{e}_b]\, (\boldsymbol{\nu}).$$

The vector auto-correlation is given by

$$[\mathbf{e}_b \star \mathbf{e}_b](\boldsymbol{\nu}) = \int_{\mathbb{R}^2} d\boldsymbol{r}_b \mathbf{e}_b^T(\boldsymbol{r}_b) \mathbf{e}_b(\boldsymbol{r}_b + \boldsymbol{\nu})$$

where $\cdot^T$ denotes the transpose operator. To find the OTF we need to evaluate the vector auto-correlation of the electric field in the back focal plane then take the angular Fourier transform of the result.

TODO: The auto-correlation calculation is in progress. I should be able to find an analytic formula for the OTF, but for now I am plotting it numerically in Figure 3.

TODO: Plot PSFs and OTFs numerically without the paraxial approximation.

TODO: Consider detection polarizers.

TODO: Consider illumination polarizers.

5 Conclusions

TODO

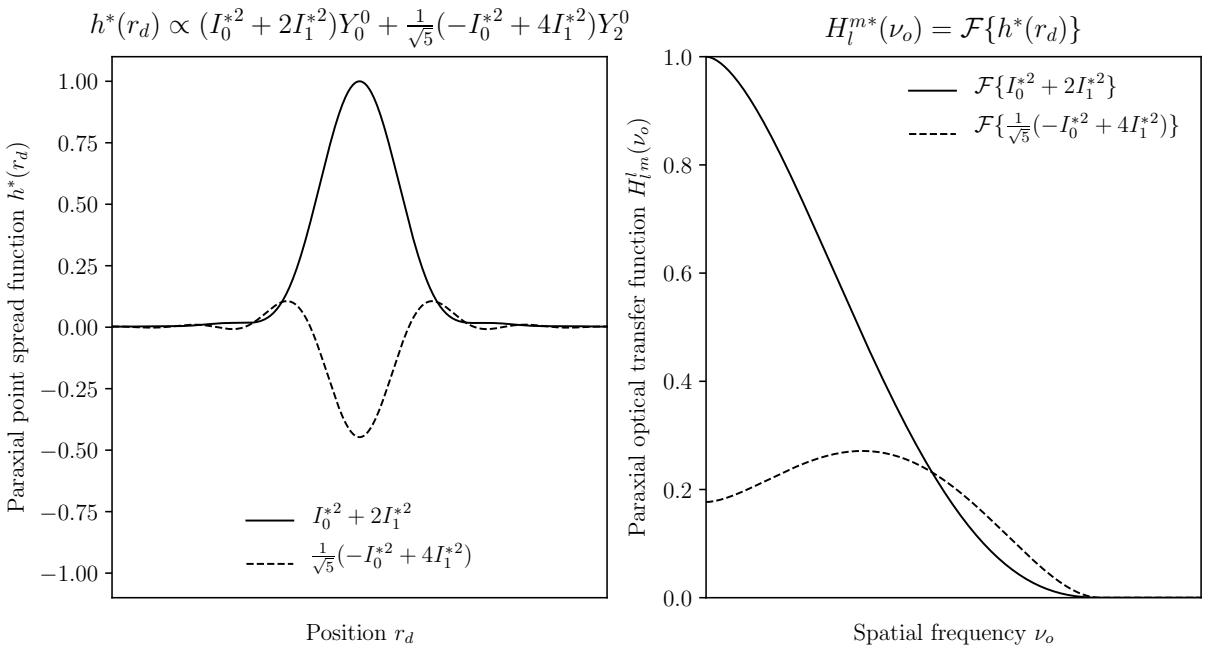

Figure 3: **Left:** Paraxial spatio-angular point spread function for a single-view fluorescence microscope with NA=0.8. The solid line is the PSF for Y_0^0 distributions and the dashed line is the PSF for Y_2^0 distributions. Y_2^0 includes "negative" fluorophores, so it gives rise to a negative PSF. **Right:** Numerical paraxial spatio-angular optical transfer function for the same microscope. The Y_0^0 term has a spatial low-pass reponse while the Y_2^0 term has a spatial high-pass response. The relative sizes of the two terms is set by the NA—increasing the NA increases the relative size of the Y_0^2 term. Vertical scaling is correct—horizontal scaling is in progress. The cutoff frequency is proportional to NA and is the same for both spherical harmonic terms.

References

[1] Adam S. Backer and W. E. Moerner. Extending single-molecule microscopy using optical Fourier processing. *J. Phys. Chem. B*, 118(28):8313–8329, 2014.

[2] Lukas Novotny and Bert Hecht. *Principles of Nano-Optics*. Cambridge University Press, 2006.

[3] J.W. Goodman. *Introduction to Fourier Optics*. MaGraw-Hill, 2nd edition, 1996.

[4] A. Papoulis and S. U. Pillai. *Probability, Random Variables, and Stochastic Processes*. McGraw-Hill Higher Education, 4 edition, 2002.

[5] J. Mertz. *Introduction to Optical Microscopy*. W. H. Freeman, 2009.